metals

MDPI

Article

Temperature-Dependent Hydrogen Embrittlement of Austenitic Stainless Steel on Phase Transformation

Young-Hwan Choi [1], Jung Hee Lee [2], Seok-Min Kim [1], Dong-Ha Lee [1], Hee-Tae Kim [1], Jeong-Hyeon Kim [3], Minjung Kim [3], Seul-Kee Kim [3,*] and Jae-Myung Lee [1,3,*]

[1] Department of Naval Architecture and Ocean Engineering, Pusan National University, Busan 46241, Republic of Korea
[2] Offshore Industries R&BD Center, Korea Research Institute of Ships and Ocean Engineering (KRISO), Geoje-si 53201, Republic of Korea
[3] Hydrogen Ship Technology Center, Pusan National University, Busan 46241, Republic of Korea
* Correspondence: skkim@pusan.ac.kr (S.-K.K.); jaemlee@pusan.ac.kr (J.-M.L.)

Abstract: A critical issue that needs to be addressed for wider utilization of hydrogen as fuel is protection against hydrogen embrittlement during cryogenic storage as it weakens the microstructure bonding force of metals through hydrogen penetration. Austenitic stainless steel, which is usually used in cryogenic vessels and is well known for its high hydrogen resistance at room temperature, has also been reported to be vulnerable to hydrogen embrittlement under cryogenic temperatures. In addition, because large storage vessels are operated over a wide range of temperatures, material behavior at various temperature conditions should also be considered. Therefore, in the present study, hydrogen charging of austenitic stainless steel was performed under various temperature conditions for carrying out prestrain and tensile tests. A decrease in the tensile strength and elongation and an increase in the yield strength were observed in all cases. In particular, the case of 20% prestrain at cryogenic temperature followed by tensile test at room temperature after hydrogen charging showed fracture in the elastic region. The hydrogen index was evaluated from the perspective of elongation and reduction in area, which are factors that indicate the degree of ductility. The aforementioned case showed the most severe results, while non-prestraining followed by tensile tests at room temperature was the least effected by hydrogen. In addition, the effect of strain-induced martensite on hydrogen embrittlement was analyzed using electron backscattered diffraction (EBSD). It was observed that the higher is the prestrain at cryogenic temperatures, the greater is the volume fraction of α′ martensite, which leads to hydrogen embrittlement. The edges and center of the fracture surface were analyzed using scanning electron microscopy (SEM). The hydrogen-charged specimens exhibited brittle fractures at the edges and ductile fractures at the center. The more severe the embrittlement, the more were the number of intergranular fractures and microdimples observed at the edges.

Keywords: liquid-hydrogen storage; hydrogen embrittlement; prestrain effect; transformation-induced plasticity; hydrogen index

check for updates

Citation: Choi, Y.-H.; Lee, J.H.; Kim, S.-M.; Lee, D.-H.; Kim, H.-T.; Kim, J.-H.; Kim, M.; Kim, S.-K.; Lee, J.-M. Temperature-Dependent Hydrogen Embrittlement of Austenitic Stainless Steel on Phase Transformation. *Metals* **2023**, *13*, 35. https://doi.org/10.3390/met13010035

Academic Editor: Francesco Iacoviello

Received: 3 November 2022
Revised: 18 December 2022
Accepted: 19 December 2022
Published: 23 December 2022

Copyright: © 2022 by the authors. Licensee MDPI, Basel, Switzerland. This article is an open access article distributed under the terms and conditions of the Creative Commons Attribution (CC BY) license (https://creativecommons.org/licenses/by/4.0/).

1. Introduction

Hydrogen is a clean and sustainable energy source that is currently considered to be one of the best potential substitutes to fossil fuels. It has thus attracted considerable attention from the transportation sector to achieve carbon neutrality. Hydrogen is not only the most abundant chemical element in the universe, but its use as an energy source results in zero greenhouse emissions, with water being the only by-product. It also has an exceptionally high gravimetric energy density of (20 kJg^{-1}), which is almost three times that of gasoline and seven times that of other fossil fuels [1]. With regard to hydrogen storage, safety and efficiency as well as easy access are key. Therefore, the storage and transportation of hydrogen plays an important role in hydrogen economics. Despite its

advantages, it is not easy to use utilize hydrogen as fuel because, it becomes very difficult to store it for transportation and utilization after its production. Further, hydrogen has a low volumetric energy density in its pure form. To resolve the limitations of hydrogen storage, there are three options: physical storage as compressed gas, physical storage as cryogenic liquid hydrogen, and solid-state storage methods.

In recent times, compressed hydrogen has been adopted owing to its moderate storage environment conditions and relatively simpler design considerations in terms of materials and structures. However, physical storage as cryogenic liquid hydrogen may be commonly adopted in the future because the density of hydrogen stored in liquid form is greater than that of compressed hydrogen; it thus stores more energy per unit volume. We base this assumption using the example of natural gas. In the past, when storing and transporting natural gas, compressed storage under high pressure was used. However, later liquefied storage methods were developed for economic and safety reasons.

To store liquid hydrogen, the most important factor in the development of liquid-hydrogen storage tank is structural safety because liquid hydrogen is stored at temperature below 20 K. In addition, as the metallic material is in direct contact with liquid hydrogen, the issue of hydrogen embrittlement must also be considered, which is a physical phenomenon that decreases ductility of metals through hydrogen penetration. Hence, the safety of liquid-hydrogen storage systems can be ensured by selecting the appropriate structure and materials. Figure 1 shows a representative liquid-hydrogen carrier equipped with a liquid-hydrogen cargo containment system. As shown in the figure, the liquid-hydrogen cargo containment system comprises a primary barrier and insulation panels that help maintain the cryogenic temperature (20 K) required for storing liquid hydrogen. The surface of the insulation panels is covered with a thin, corrugated stainless-steel layer that absorbs thermal deformations. The stainless-steel layer, which is exposed to a temperature of 20 K, is the primary barrier in a liquefied natural gas (LNG) cargo containment system (CCS). This primary barrier is shaped in the form of a corrugated sheet to enable the tank to withstand frequent changes in thermal conditions during operation.

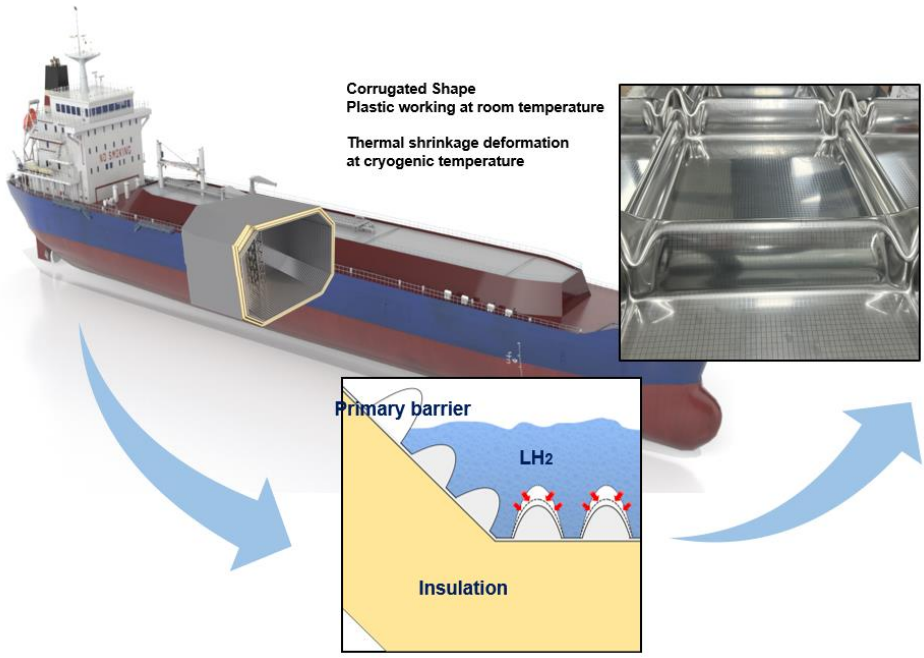


Figure 1. Schematic of membrane-type liquified hydrogen (LN2) cargo containment system.

As the material used for the primary barrier must exhibit superior mechanical performance at low temperatures, austenitic stainless steel is generally preferred. This is because it is well known as a high-hydrogen-resistance material and is frequently used in cryogenic storage vessels and pipelines because of its stability and high elongation at low tempera-

tures. However, it is susceptible to transformation-induced plasticity (TRIP) at low temperatures. Because TRIP steel has a low stacking fault energy, phase transformation occurs under a low-temperature tensile load from the fully austenitic phase at room temperature. The face-centered cubic (FCC) austenite phase forms body-centered cubic (BCC) α′-martensite directly or via hexagonal close-packed (HCP) ε-martensite [2–5]. This is because stacking faults have adequate space for ε-martensite, and α′-martensite nucleates and grows in pile-up dislocations [6,7]. This phenomenon depends on temperature—transformation to martensite increases with decrease in temperature; thus, the material strengthens with a drop in temperature [8,9].

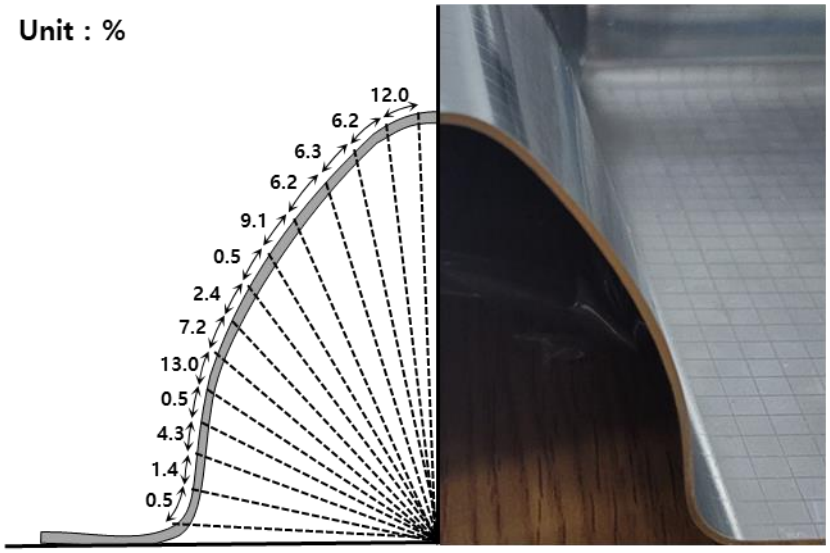
However, this phase transformation can be dangerous in case of hydrogen embrittlement. Wang et al. found that in the case of prestrained austenitic stainless steel, because the effect of dislocation density is lower than that of martensite, the effect of martensite is dominant to hydrogen embrittlement [10]. In the hydrogen environment, austenite has a high solubility of hydrogen compared to α′-martensite, while α′-martensite has high diffusivity and permeability [11–13]. In addition, when hydrogen-containing austenite transforms into martensite, hydrogen solubility is transferred to austenite. At this time, α′-martensite not only acts as a "highway" for transporting hydrogen but also promotes crack initiation between martensite-rich and austenite-rich regions [14–16].

For shaping the primary barrier in the form of a corrugated sheet, a flat-type plate is folded using a metal press operating at ambient temperature. This pressing process induces a significant prestrain in the corrugated sheet. That is, the degree of phase transformation varies according to the degree of prestrain of the curvature, which means that the region of the primary barrier that has experienced prestrain may have a lower resistance to hydrogen charging compared to the region that has not experienced it. Thus, it is essential to evaluate the effect of hydrogen on exposure to various temperatures and loading conditions owing to the nature of sea transportation, where the loading and unloading of liquid hydrogen is performed repeatedly, and the vessel moves in six degrees of freedom. However, research on hydrogen embrittlement and preliminary strain by temperature in relation to liquid-hydrogen CCSs is scarce.

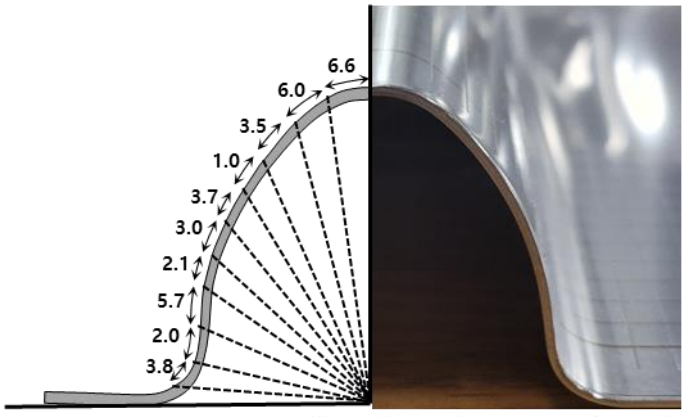
Figure 2 shows the degree of prestrain on the corrugated steel membrane of the liquefied hydrogen carrier cargo containment system. As shown in this figure, each part undergoes different degrees of strain in the process of press working during fabrication to improve the mechanical and thermal performance of the primary barrier. Prestraining of the primary barrier has a large range of deformation between <1% and 13%. Although the figure shows only the large and small corrugation parts, the degree of prestrain exceeds over 20% once the knot part is considered. In recent decades, the effects of prestraining on hydrogen embrittlement of stainless steel has been investigated. Zhou et al. investigated the effect of prestraining on the hydrogen embrittlement of austenitic stainless steel under different hydrogen conditions. Tensile tests were conducted under cathodic-hydrogen-, gaseous-hydrogen-, and hydrogen-charged conditions. In the case of hydrogen-charged electrochemical surface, the hydrogen embrittlement susceptibility increased slowly and then increased rapidly with increasing prestrain. In addition, in the gaseous-hydrogen environment, hydrogen embrittlement susceptibility increased and then decreased with increasing prestrain [17]. Kim et al. (2016) reported the effects of phase transformation and hydrogen embrittlement for 304 stainless steel. Room-temperature tensile tests were conducted at different strain rates on hydrogen-free and hydrogen-charged 304 stainless steel. The results showed that the ductility, tensile stress, and strain-induced martensite content increased with decreasing strain rate in hydrogen-free 304 stainless steel, but decreased in hydrogen-charged 304 stainless steel [18].

Although certain studies have investigated the correlation between prestraining and hydrogen embrittlement, most of them so far are limited to the observation of simple material changes and do not consider the actual production and application environments. Moreover, despite the clear influence of temperature, most studies so far have focused on the effect of prestrain at only room temperature. Although certain studies considering

the prestrain environment for the low-temperature region have been reported in literature related to LNG storage and transportation, LNG does not have an effect similar to hydrogen embrittlement; therefore, the results of these studies are limited in their direct application to liquid-hydrogen storage tanks. For this reason, this study was conducted to investigate the correlation between prestrain temperature, hydrogen charging, environment, and temperature region to which a load is applied for austenitic stainless steel, which acts as the primary barrier during the storage and transportation of liquid hydrogen. Both parts of the primary barrier have a large range of deformation owing to plastic working at room temperature. This shape effectively resists heat shrinkage and improves fatigue performance.



(**a**)



(**b**)

Figure 2. The degree of prestrain on the (**a**) large corrugation part and (**b**) small corrugation part.

2. Materials and Methods

Table 1 lists the chemical composition of the investigated 304L stainless steel, which is a representative TRIP steel with high elongation and strength at low temperatures. This type of material is used in cryogenic liquid storage systems such as storage of LNG at 110 K and that of liquid hydrogen at 20 K temperature. In the present study, test samples were obtained from the material of actual membrane-type primary barrier of the storage system. Figure 3 shows the shape and dimensions of the tested sample. The overall length and gauge length of the testing sample were 100 and 25 mm, respectively. In addition, the width and thickness of the testing sample were 6.5 and 2 mm, respectively.

Table 1. Chemical composition of the SUS304L used in this study (wt. %).

Composition	C	Si	Mn	P	S	Ni	Cr	Mo	Fe
SUS304L	0.018	0.4	1.63	0.03	0.001	8.2	18.1	0.22	Bal.

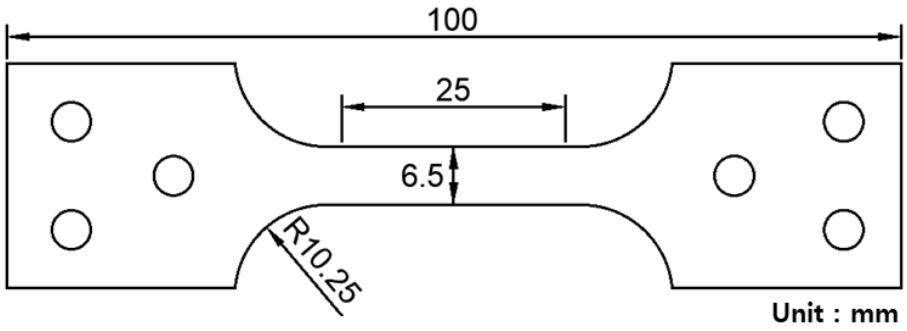


Figure 3. Shape and dimension of the flat-type experimental specimen made of SUS 304L stainless steel.

The cathodic charge method proposed by ISO-16573 was used before the tensile tests. According to the ISO code, for a large amount of hydrogen charging, the chemical composition ratio of the aqueous solution used in this process should be 30 g/L NaCl and 3 g/L NH4SCN. A platinum mesh was connected to the anode and a tensile specimen was connected to the cathode. Wang et al. have shown that with respect to charging time and current density, as hydrogen is charged, hydrogen concentration initially increases rapidly and then becomes constant after a certain period of time and density. They explained that this is because hydrogen gradually penetrates the steel from the surface, and further diffusion becomes difficult and time consuming. [19]. Therefore, a current density of 20 mA/cm^2 was applied for 72 h using a constant-current-supply device. To carry out the prestrain and tensile tests, a universal test machine (KSU-5 M, Kyoungsung, Ansan, Republic of Korea) and cryogenic chamber (digital control method in the range of −200 °C to 100 °C) were used. To maintain the cryogenic temperature, the flow of cryogenic nitrogen gas was purged directly using a relay controller. For accurate strain data acquisition, a cryogenic extensometer (3542-050M-100-LT, Epsilon Tech, Jackson, WY, USA) was attached to the specimens. To evaluate the effect of prior transformation on hydrogen embrittlement, the phases of the prestrained specimens were observed using electron backscattered diffraction (EBSD; Mira 3 LMH In-Beam, TESCAN, Brno, Czech Republic). The mounted specimens were ground and polished using 400–4000 grit sandpapers, 3 μm and 1 μm polycrystalline diamond, and 0.05 μm alumina powder.

In this study, the mechanical behavior under various temperature conditions and hydrogen environments was evaluated. Hydrogen charging was performed after applying the same- or alternating-temperature conditions in the prestrain and tensile tests. The temperature conditions were room temperature and cryogenic temperature, and the prestrain conditions were 0%, 10%, and 20%. The cryogenic temperature was selected to be 77 K, as it has been reported that the maximum volume fraction of α'-martensite occurs near 77 K [20,21]. The test method followed ASTM E8 with a strain rate of 0.2/min. Each condition was tested 3–5 times in order to ensure repeatability. The scenarios are summarized in Table 2. The first letter of the notation for the scenario refers to the temperature condition of the prestrain while the second letter indicates the temperature condition of the tensile test. Here, R and C refer to the room and cryogenic temperatures, respectively. The numbers after the temperature conditions indicate the degree of prestrain; however, for non-prestrained specimens, the same letters are indicated. In addition, whether hydrogen is charged or not is indicated by H or N in brackets.

Table 2. Experimental scenarios.

Case	Temperature of Prestrain	Degree of Prestrain	Temperature of Tensile Test	Hydrogen Charging
1	Room Temperature	0	Room Temperature	Hydrogen Charging or not
2		10		
3		20		
4	Cryogenic Temperature	0	Cryogenic Temperature	
5		10		
6		20		
7	Room Temperature	10	Cryogenic Temperature	
8		20		
9	Cryogenic Temperature	10	Room Temperature	
10		20		

3. Results and Discussion

304L stainless steel at room temperature is fully austenitic. However, phase transformation from fully austenite to martensite occurs as the temperature decreases under tensile load owing to the relatively low stacking fault energy of the steel. Specifically, the fraction of ε-martensite increases to a maximum and decreases thereafter, and α'-martensite increases continuously [8]. Even though dislocations and twins are also generated under tensile loads and affect hydrogen embrittlement, it is well known that the influence of α'-martensite on hydrogen embrittlement is dominant compared to other causes [10].

The results are presented in Figure 4 and Table 3. Fe-FCC and Fe-BCC indicate austenite and α'-martensite, respectively. In the case of nonprestrained specimens, the ratio of austenite and martensite was measured to be 90.86% and 9.14%, respectively. The ratio between austenite and martensite in the prestrained specimens at room temperature was almost unchanged at 88.3%:11.7% at 10% prestrain and 87.87%:12.13% at 20% prestrain. However, at cryogenic temperatures, the martensite ratio rapidly increased to 17.89% and 82.11%, respectively.

The results of the prior deformation define the degree of hydrogen effect. The hydrogen diffusivity and permeability of α'-martensite are several orders of magnitude higher than those of austenite [16,22]. In other words, α'-martensite plays a role in enhancing the hydrogen transport rate and hydrogen uptake during hydrogen charging [10].

Table 3. Volume fraction of prestrained specimens.

Prestrain	Non	R 10	R 20	C 10	C 20
FCC (%)	90.86	88.30	87.87	80.93	17.89
BCC (%)	9.14	11.70	12.13	19.07	82.11

3.1. Stress-Strain Relationship

The shape of the graphs was determined based on whether secondary hardening owing to phase transformation is clearly visible, depending on the temperature condition of the tensile test.

As shown in Figure 5, the higher stacking fault energy of austenite at room temperature leads to homogeneous dislocation and shows the behavior of general ductile steel. However, the behavior at 77 K shows clear secondary hardening. Unlike the room-temperature condition, not only does it enhance the dislocation density, but phase transformation from γ to α' also occurs because of the low stacking fault energy at the cryogenic temperature [2,3]. This is the reason for the maintenance of a high elongation compared to other materials at cryogenic temperatures.

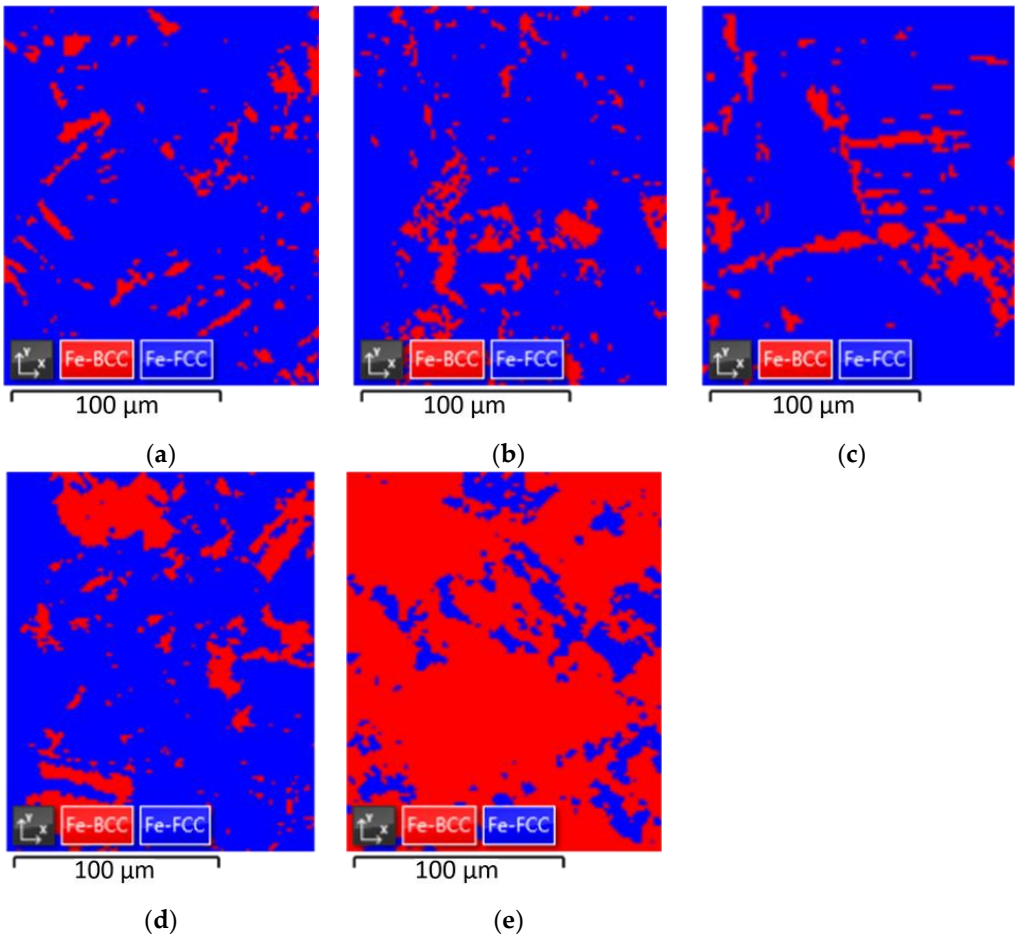


Figure 4. EBSD maps: (**a**) non-prestrained specimen, (**b**) 10% prestrained specimen at room temperature, (**c**) 20% prestrained specimen at room temperature, (**d**) 10% prestrained specimen at cryogenic temperature, and (**e**) 20% prestrained specimen at cryogenic temperature.

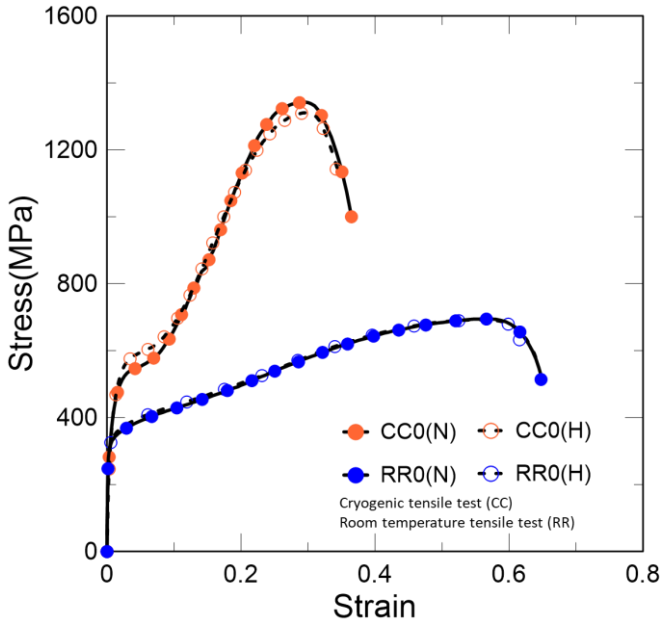


Figure 5. Stress–strain curves at cryogenic and room temperatures. CC0 and RR0 denote cryogenic and room temperatures, respectively. (H) and (N) represent whether hydrogen is charged or not, respectively.

Both cases were charged in a fully austenitic state, and these results indicate the tensile behavior under different temperature conditions after hydrogen charging. According to these results, the phase transformation after hydrogen charging does not have a significant effect on hydrogen embrittlement.

3.2. Mechanical Characteristics

As shown in Table 4 and Figure 6a, the specimens under this condition exhibited the highest hydrogen embrittlement resistance among all scenarios. The non-prestrained and 10% prestrained specimens have almost in the same yield strength irrespective of hydrogen charging, whereas the 20% prestrained specimen increased by 4.5%. Regarding tensile strength, the non-prestrained specimen was not affected by hydrogen charging, but the 10% and 20% prestrained specimens showed a decrease of 2.3% and 2.7%, respectively. The elongation, according to the degree of prestrain, decreased by 0.8%, 3.7%, and 12.3%, respectively. In other words, changes in mechanical properties due to hydrogen charging are proportional to the degree of prestrain. As shown in Figure 4a, it can be concluded that in these cases, the hydrogen resistance is relatively strong as austenite occupies most of the phases, and as shown in Figure 4b,c, the degree of hydrogen embrittlement increases as the ratio of α'-martensite increases. However, as mentioned by Spencer et al., strain-induced martensite increase owing to prestrain is too small to lead to a slight difference in mechanical behaviors at room temperature [23].

Hydrogen embrittlement is generally explained by hydrogen-enhanced strain-induced vacancy formation (HESIV), hydrogen-induced decohesion (HID), absorption-induced dislocation emission (AIDE), and hydrogen-enhanced local plasticity (HELP) [24,25].

HESIV theory describes this behavior as hydrogen accelerating strain-induced vacancy formation and stabilizing vacancy clusters. As a result, void initiation and premature failure occur, which reduces the ductile crack resistance and causes embrittlement [26,27]. According to HID theory, hydrogen reduces metal atomic cohesion, thereby increasing the risk of decohesion between atoms under lower tensile stress and embrittlement [28]. As per the AIDE theory, the adsorption of hydrogen weakens the interatomic bonds and promotes dislocation emission at the crack tips, resulting in a rapid increase in the dislocation density and mobility. This phenomenon grows with the crack opening, and eventually the coalescence of cracks with voids occurs at a lower strain [27]. According to the HELP theory, the shielding effect of dislocations by hydrogen on the elastic stress field enhances the mobility of dislocations and slip localization. This enhances plasticity and reduces resistance to stress [29–31]. Despite these theories, the reason for the increase in the yield strength of the hydrogen-charged specimen in this experiment is that the hydrogen-induced mechanical behavior depends on the strain rate. Bak et al. reported that after a certain strain rate, the yield strength of a charged specimen is greater than that of an uncharged specimen [32,33].

Under isothermal deformation at 77 K, because prior α'-martensite increases the hydrogen effect, prestrained specimens fractured before the necking region, as shown in Table 4 and Figure 6b. In each case, the yield strength increased by 14.1%, 14.7%, and 16.6%, in the order of non-prestrained, 10%, and 20%, respectively, while the elongation decreased by 5.0%, 50.7%, and 84.5%, respectively. In addition to the causes behind Case 1 behavior, the increase in yield strength in this case occurs because the plastic deformation owing to dislocation mobility appears smaller at 77 K than that at room temperature. However, the shielding effect of hydrogen mentioned in the HELP theory appears only when hydrogen is transported by dislocations; thus, the shielding effect is hardly expected at cryogenic temperatures [31,34].

The behavior of Cases 7 and 8 is different from that of the previous cases. In the prestrained specimen, martensite transformation occurred rapidly and propagated along the tensile direction [23]. At that time, as shown in Figure 6c, after the load drop, a plateau region appeared, which was shortened by hydrogen charging. The tensile strength and elongation of the 10% prestrained specimen with more deformation at cryogenic

temperatures were higher than those of the 20% prestrained specimen. As shown in Table 5, with hydrogen charging, the yield strengths of the 10% and 20% prestrained specimens increased by 1.5% and 13.4%, respectively. The tensile strengths decreased by 1.5% and 5.7% and the elongations decreased by 3.3% and 14.0%, respectively. Compared with Cases 1–3, which have the same prestrain temperature, many studies have reported that strain-induced martensite affects hydrogen embrittlement; however, hydrogen itself does not affect the phase transformation [35,36]. Therefore, none of the cases showed a severe hydrogen effect. Compared with Cases 4–6, which have the same tensile test temperature, specimens with less prior α'-martensite at room temperature can prevent hydrogen embrittlement.

As shown in Figure 6d and Table 5, in the case of prestraining at 77 K followed by tensile test at room temperature, secondary hardening is not clear, which is the condition most vulnerable to hydrogen embrittlement. The austenite structure at cryogenic temperatures consists of partial dislocations and extended stacking faults. After sufficient strain at cryogenic temperatures, this structure remained stable under tensile loads at room temperature. In this process, a large number of potent nucleation sites for martensite are generated, and martensite is transformed rapidly [23]. Thus, Cases 9 and 10 represent the most severe conditions that also affect hydrogen embrittlement. The yield strength of the 10% prestrained specimen increased by 5.1%, whereas its tensile strength and elongation decreased by 17.7% and 71.9%, respectively. However, in the case of the 20% prestrained specimen, the elongation decreased by 95.2% and the specimen fractured before the yield point.

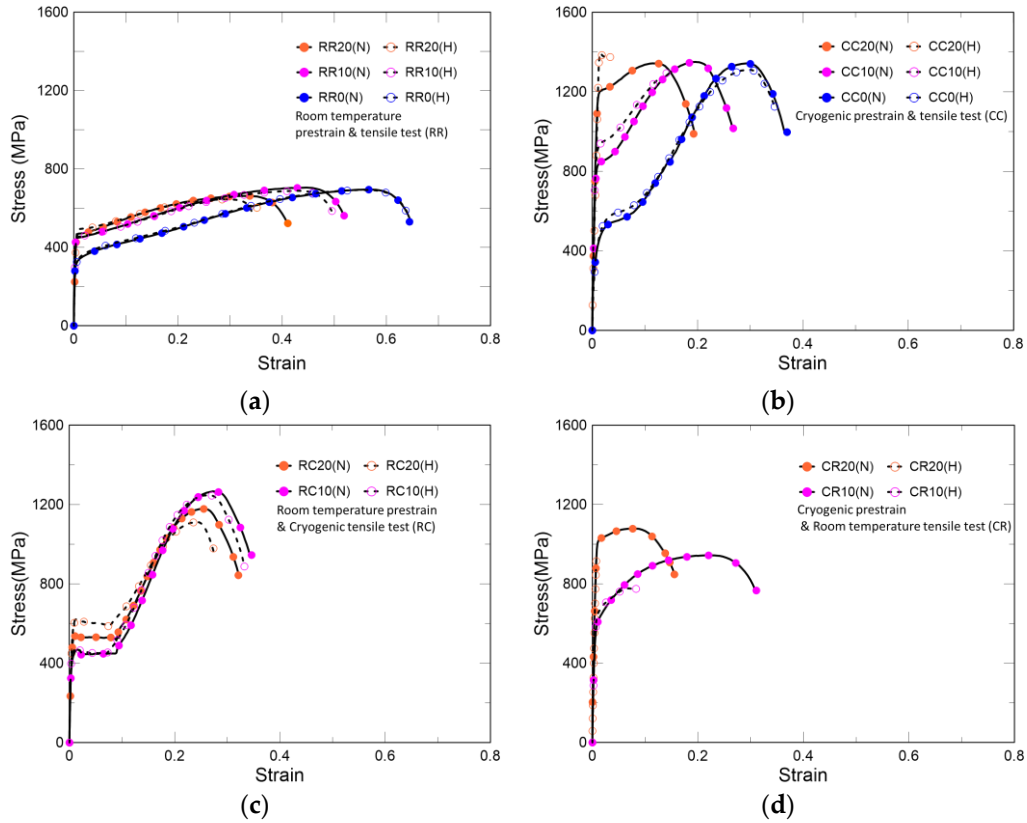


Figure 6. Stress–strain curves: (**a**) isothermal deformation at room temperature, (**b**) isothermal deformation at 77 K, (**c**) prestrain at room temperature followed by tensile test at 77 K, (**d**) prestrain at 77 K followed by tensile test at room temperature. R and C refer to the room and cryogenic temperatures, respectively. The former letter denotes the temperature of prestrain, while the latter represents the temperature of the tensile test. The numbers after the temperature conditions indicate the degree of prestrain; however, for nonprestrained specimens, the same letters are used. In addition, whether hydrogen is charged or not is indicated by H or N in brackets, respectively.

Table 4. Material properties of isothermal deformation at room temperature and cryogenic temperature.

Temperature	Prestrain	Hydrogen Uncharged			Hydrogen Charged		
		Yield Strength (MPa)	Tensile Strength (MPa)	Elongation (%)	Yield Strength (MPa)	Tensile Strength (MPa)	Elongation (%)
RR	Non	295	695	65.0	298	693	64.5
	10	449	705	51.9	454	689	50.0
	20	469	663	41.1	490	645	36.1
CC	Non	280	1343	36.5	320	1312	34.7
	10	810	1351	27.0	929	1278	13.3
	20	1195	1344	19.5	1393	1397	3.0

Table 5. Material properties of different temperature conditions between prestrain and tensile tests.

Temperature	Prestrain	Hydrogen Uncharged			Hydrogen Charged		
		Yield Strength (MPa)	Tensile Strength (MPa)	Elongation (%)	Yield Strength (MPa)	Tensile Strength (MPa)	Elongation (%)
RC	10	446	1267	34.4	452	1248	33.3
	20	531	1180	32.2	603	1112	27.7
CR	10	603	945	31.0	634	778	8.7
	20	1017	1080	15.7	-	948	0.8

3.3. Hydrogen Index

Although not a design parameter, reduction in area is one indicator to quantitatively evaluate the degree of ductility with elongation; it is obtained by dividing the reduction in the fracture surface by the initial cross-sectional area. As shown in Tables 6 and 7 as well as Figure 7, all hydrogen-charged specimens exhibited a decrease the reduction in area. The specimens that were prestrained at cryogenic temperatures showed a lower reduction in area than those prestrained at room temperature. That is, in terms of reduction in area, the higher prior α'-martensite is the more severe for hydrogen embrittlement.

To evaluate the hydrogen index, that is, the ductility loss index, the reduction in area and elongation were used as the main indicators. They are defined as follows [19,29]:

$$\delta_L = (\delta_0 - \delta_H)/\delta_0, \quad (1)$$

$$\varphi_L = (\varphi_0 - \varphi_H)/\varphi_0 \quad (2)$$

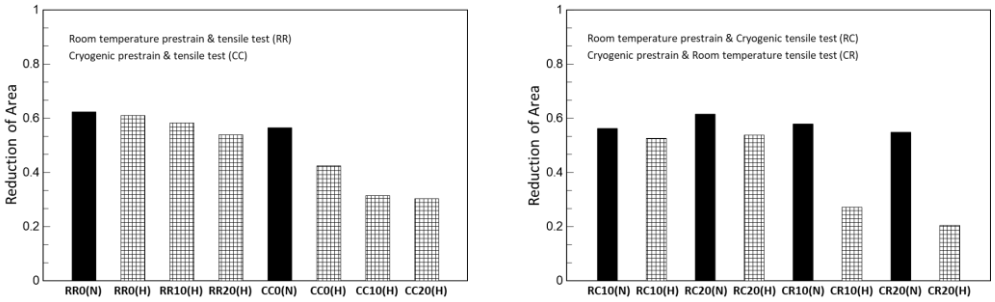
where δ_0 and φ_0 are respectively the elongation and reduction in the area of the hydrogen-uncharged specimens, and δ_H and φ_H are the elongation and reduction in the area of the hydrogen-charged specimens, respectively. The hydrogen index of the specimens prestrained at cryogenic temperature was higher than that at room temperature, and as the prestrain increased, the hydrogen index increased. Overall, the comparison of δ_L and φ_L was different for each case, as shown in Figure 8 and Table 7. The values of the specimens prestrained at cryogenic temperatures are higher than those prestrained at room temperature. Austenitic stainless steel has high hydrogen resistance at room temperature, as shown by its low hydrogen index. However, specimens prestrained at cryogenic temperatures lost ductility over 40%, and the CR20 specimen had the highest value from both points of view. Thus, it can be said to have the highest susceptibility to hydrogen. Therefore, deformation at cryogenic temperatures in liquefied hydrogen storage tanks should be considered from the design stage itself.

Table 6. Reduction in area under the same-temperature condition between prestraining and tensile test.

	RR0(N)	RR0(H)	RR10(H)	RR20(H)	CC0(N)	CC0(H)	CC10(H)	CC20(H)
RA	0.62	0.61	0.58	0.54	0.56	0.42	0.31	0.30

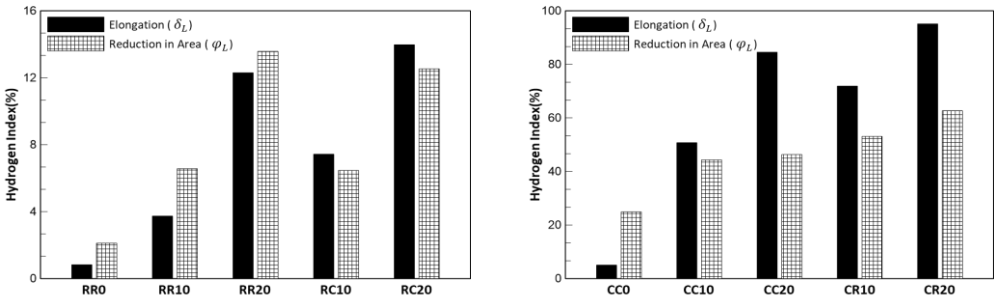
Table 7. Reduction in area under the alternating-temperature condition between prestraining and tensile test.

	RC10(N)	RC10(H)	RC20(N)	RC20(H)	CR10(N)	CR10(H)	CR20(N)	CR20(H)
RA	0.56	0.53	0.62	0.54	0.58	0.27	0.55	0.20



(**a**) (**b**)

Figure 7. Reduction in area: (**a**) the same-temperature condition between prestrain and tensile test and (**b**) the alternating-temperature condition.



(**a**) (**b**)

Figure 8. Hydrogen index: (**a**) prestrained at room temperature and (**b**) prestrained at cryogenic temperature. The elongation and reduction in area show different tendencies; however, the condition of prestrain at cryogenic temperatures is higher than that at room temperature. In addition, the cases with a high hydrogen index show higher elongation than reduction in area.

3.4. Fracture Surface

Because hydrogen is charged from the edges to the center, the fracture surface exhibits different features between these two regions. As shown in Figure 9, both points on the fracture surfaces were analyzed using scanning electron microscopy (SEM). At the edges of all hydrogen-charged specimens, transgranular fractures by martensite, flat facets and secondary cracks by twin boundaries, and relatively small dimples were observed [37]. The more severe the degree of embrittlement, the greater was the proportion of intergranular fractures from hydrogen-enhanced plasticity processes [38]. In particular, in the case of CR20(H), brittle fracture was observed up to the center of the surface. Except for CR20(H), the hydrogen-charged specimens exhibited ductile failure characterized by dimples toward the center, as shown in Figure 9d. On the contrary, the uncharged specimens showed ductile fractures, such as shear dimples at the edges and dimples at the center, as shown in Figure 10a,b.

Three main theories (HID, HELP, and AIDE) can be used to explain hydrogen-induced cracking for different fracture morphologies. As mentioned in the HID theory, this feature is noticeable in vulnerable regions, such as grain boundaries, because of the increased risk of decohesion due to the decreased bonding energy between atoms when hydrogen is charged [38,39]. As per AIDE theory, because dislocation loops are nucleated and expanded at the crack tip along the slip plane, a smaller plastic zone is formed, and the shape of the

fracture becomes sharp rather than blunt. Therefore, this phenomenon creates shallow and small dimples on transgranular and intergranular fractures [25]. According to HELP theory, hydrogen atoms locally enhance the mobility of dislocations. Around this region, deformation by shear stress occurs and microvoids are generated. During the coalescence of the microvoids, microcracks occur simultaneously, which lead to creation of small dimples [40].

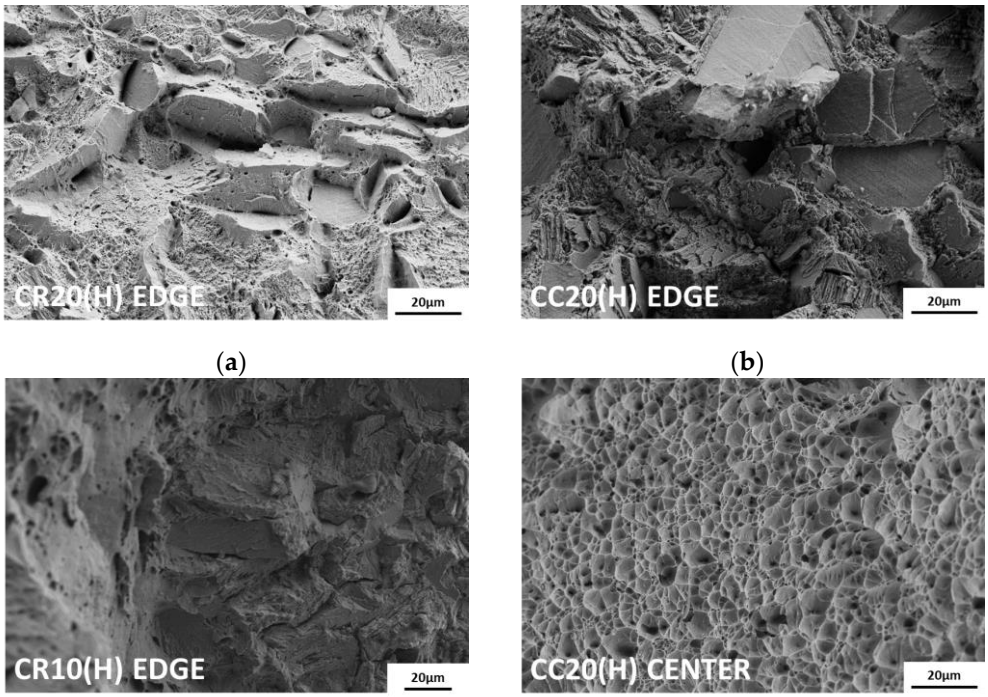


Figure 9. Fracture surface: (**a**) edge of CR20(H), (**b**) edge of CC20(H), (**c**) edge of CR10(H), and (**d**) center of CC20(H). At the edges of all hydrogen-charged specimens, brittle fractures such as transgranular fractures, intergranular fractures, flat facets, and secondary and micro dimples are observed. At the center, the hydrogen-charged specimens show ductile failure.

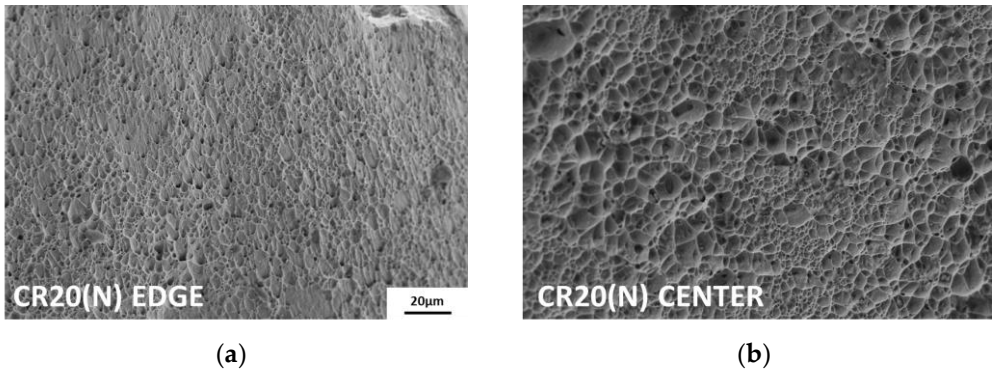


Figure 10. Fracture surface: (**a**) edge of CR20(N) and (**b**) center of CR20(N).

4. Concluding Remarks

This study investigated the effect of hydrogen charging according to temperature and prestrain conditions on the tensile behavior of SUS304L. The results of this study can provide practical data on hydrogen embrittlement for consideration in the development and design of large-sized liquefied hydrogen storage vessels. The main conclusions are as follows:

- From the EBSD observation, nonprestrained SUS304L testing samples with austenitic phase showed insignificant effects of hydrogen charging.
- In the stress–strain relationship with hydrogen charging, the prestrain temperature affected the reduction in elongation. In contrast, the experimental temperature affected the general shape of the stress–strain relationship.
- The CR20(H) case, which involves 20% prestraining at cryogenic temperature followed by testing at room temperature, showed the most extreme results, with fracture in the elastic region owing to hydrogen embrittlement.
- In all cases, the yield strength increased, whereas the tensile strength and elongation decreased owing to hydrogen charging.
- The hydrogen index, which represents the hydrogen susceptibility of metallic materials, was proposed. Using it, the temperatures and degree of prestrain considered hydrogen index can be available.
- Transgranular fractures, flat facets, and secondary cracks on the edges were observed in the samples with hydrogen charging. In addition, dimples, which are a primary indicator of ductile fracture, were observed at the center of the fracture surfaces in all specimens, except for CR20.

Author Contributions: Conceptualization, Y.-H.C., H.-T.K. and J.H.L.; investigation, S.-M.K., D.-H.L. and H.-T.K.; writing—original draft preparation, Y.-H.C., J.-H.K. and J.-M.L.; data curation, S.-K.K., M.K. and Y.-H.C.; writing—review and editing, M.K., D.-H.L. and J.-H.K.; visualization, Y.-H.C., J.H.L., S.-M.K. and J.-M.L.; supervision, J.-M.L. and S.-K.K. All authors have read and agreed to the published version of the manuscript.

Funding: This research was supported by Korea Research Institute of Ships and Ocean engineering a grant from Endowment Project of "Topside platform basic design on concentrated floating-type offshore pretreatment process, and core technology development for liquid hydrogen multi-layer insulation system" project (PES4364). This work was supported by the Materials/Parts Technology Development Program (20017530, Development of cryogenic insulation materials and container application/evaluation technology for liquid hydrogen storage containers for hydrogen commercial vehicles) funded by the Ministry of Trade, Industry & Energy (MOTIE, Korea). This work was supported by the Korea Institute of Energy Technology Evaluation and Planning (KETEP) and the Ministry of Trade, Industry & Energy (MOTIE) of the Republic of Korea (20224000000090).

Institutional Review Board Statement: Not applicable.

Informed Consent Statement: Not applicable.

Data Availability Statement: The data presented in this study are available on request from corresponding author.

Conflicts of Interest: The authors declare no conflict of interest.

References

1. Durbin, D.J.; Malardier-Jugroot, C. Review of Hydrogen Storage Techniques for on Board Vehicle Applications. *Int. J. Hydrogen Energy* **2013**, *38*, 14595–14617. [CrossRef]
2. Pan, C.; Chu, W.Y.; Li, Z.B.; Liang, D.T.; Su, Y.J.; Gao, K.W.; Qiao, L.J. Hydrogen Embrittlement Induced by Atomic Hydrogen and Hydrogen-Induced Martensites in Type 304L Stainless Steel. *Mater. Sci. Eng. A* **2003**, *351*, 293–298. [CrossRef]
3. Zhang, H.; Huang, C.; Huang, R.; Li, L. Influence of Pre-Strain on Cryogenic Tensile Properties of 316LN Austenitic Stainless Steel. *Cryogenics* **2020**, *106*, 103058. [CrossRef]
4. Michler, T.; Naumann, J.; Hock, M.; Berreth, K.; Balogh, M.P.; Sattler, E. Microstructural Properties Controlling Hydrogen Environment Embrittlement of Cold Worked 316 Type Austenitic Stainless Steels. *Mater. Sci. Eng. A* **2015**, *628*, 252–261. [CrossRef]
5. Talonen, J.; Nenonen, P.; Pape, G.; Hänninen, H. Effect of Strain Rate on the Strain-Induced-Martensite Transformation and Mechanical Properties of Austenitic Stainless Steels. *Metall. Mater. Trans. A* **2005**, *36*, 421–432. [CrossRef]
6. Datta, K.; Delhez, R.; Bronsveld, P.M.; Beyer, J.; Geijselaers, H.J.M.; Post, J. A Low-Temperature Study to Examine the Role of ε-Martensite during Strain-Induced Transformations in Metastable Austenitic Stainless Steels. *Acta Mater.* **2009**, *57*, 3321–3326. [CrossRef]
7. Lee, W.S.; Lin, C.F. Effects of Prestrain and Strain Rate on Dynamic Deformation Characteristics of 304L Stainless Steel: Part 2—Microstructural Study. *Mater. Sci. Technol.* **2002**, *18*, 877–884. [CrossRef]

8. Sayed, A.M.; Alanazi, H. Performance of Steel Metal Prepared using Different Welding Cooling Methods. *Case Stud. Constr. Mater* **2022**, *16*, e00953. [CrossRef]
9. Nam, Y.H.; Park, J.S.; Baek, U.B.; Suh, J.Y.; Nahm, S.H. Low-Temperature Tensile and Impact Properties of Hydrogen-Charged High-Manganese Steel. *Int. J. Hydrogen Energy* **2019**, *44*, 7000–7013. [CrossRef]
10. Wang, Y.; Wu, X.; Wu, W. Effect of A′ Martensite Content Induced by Tensile Plastic Prestrain on Hydrogen Transport and Hydrogen Embrittlement of 304L Austenitic Stainless Steel. *Metals* **2018**, *8*, 660. [CrossRef]
11. Perng, T.; Altste-M'er, J. Effects of Deformation on Hydrogen Permeation in Austenitic Stainless Steels. *Acta Metall.* **1986**, *34*, 1771–1781.
12. Wang, Y.; Wang, X.; Gong, J.; Shen, L.; Dong, W. Hydrogen Embrittlement of Catholically Hydrogen-Precharged 304L Austenitic Stainless Steel: Effect of Plastic Pre-Strain. *Int. J. Hydrogen Energy* **2014**, *39*, 13909–13918. [CrossRef]
13. Wang, Y.; Zhou, Z.; Wu, W.; Gong, J. Warm Pre-Strain: Strengthening the MetasTable 304L Austenitic Stainless Steel without Compromising Its Hydrogen Embrittlement Resistance. *Materials* **2017**, *10*, 1331. [CrossRef] [PubMed]
14. Ueki, S.; Koga, K.; Mine, Y.; Takashima, K. Crystallographic Characterisation of Hydrogen-Induced Twin Boundary Separation in Type 304 Stainless Steel Using Micro-Tensile Testing. *ISIJ Int.* **2019**, *59*, 927–934. [CrossRef]
15. Zhang, L.; Li, Z.; Zheng, J.; Zhao, Y.; Xu, P.; Zhou, C.; Li, X. Effect of Strain-Induced Martensite on Hydrogen Embrittlement of Austenitic Stainless Steels Investigated by Combined Tension and Hydrogen Release Methods. *Int. J. Hydrogen Energy* **2013**, *38*, 8208–8214. [CrossRef]
16. Wang, Y.; Wu, X.; Li, X.; Wu, W.; Gong, J. Combined Effects of Prior Plastic Deformation and Sensitization on Hydrogen Embrittlement of 304 Austenitic Stainless Steel. *Int. J. Hydrogen Energy* **2019**, *44*, 7014–7031. [CrossRef]
17. Zhou, C.; Song, Y.; Shi, Q.; Hu, S.; Zheng, J.; Xu, P.; Zhang, L. Effect of Pre-Strain on Hydrogen Embrittlement of Metastable Austenitic Stainless Steel under Different Hydrogen Conditions. *Int. J. Hydrogen Energy* **2019**, *44*, 26036–26048. [CrossRef]
18. Kim, Y.S.; Bak, S.H.; Kim, S.S. Effect of Strain-Induced Martensite on Tensile Properties and Hydrogen Embrittlement of 304 Stainless Steel. *Metall. Mater. Trans. A Phys. Metall. Mater. Sci.* **2016**, *47*, 222–230. [CrossRef]
19. Wang, Y.; Gong, J.; Jiang, Y.; Jiang, W.; Jiang, W. Ductility Loss of Hydrogen-Charged and Releasing 304L Steel. *Front. Mech. Eng.* **2013**, *8*, 298–304. [CrossRef]
20. Borchers, C.; Michler, T.; Pundt, A. Effect of Hydrogen on the Mechanical Properties of Stainless Steels. *Adv. Eng. Mater.* **2008**, *10*, 11–23. [CrossRef]
21. Pinto, H.; Pyzalla, A.R.; Hübner, W.; Mus, K.A. Influence of Environment, Temperature and Chemical Composition on the Microstructural Deterioration of CrNi Steels during Friction. *Materwiss Werksttech* **2004**, *35*, 716–721. [CrossRef]
22. San Marchi, C.; Somerday, B.P.; Tang, X.; Schiroky, G.H. Effects of Alloy Composition and Strain Hardening on Tensile Fracture of Hydrogen-Precharged Type 316 Stainless Steels. *Int. J. Hydrogen Energy* **2008**, *33*, 889–904. [CrossRef]
23. Spencer, K.K.; Véron, M.; Zhang, Y.; Embury, J.D. The Strain Induced Martensite Transformation in Austenitic Stainless Steels Part 1—Influence of Temperature and Strain History. *Mater. Sci. Technol.* **2009**, *25*, 7–17. [CrossRef]
24. Li, X.; Ma, X.; Zhang, J.; Akiyama, E.; Wang, Y.; Song, X. Review of Hydrogen Embrittlement in Metals: Hydrogen Diffusion, Hydrogen Characterization, Hydrogen Embrittlement Mechanism and Prevention. *Acta Metall. Sin.* **2020**, *33*, 759–773. [CrossRef]
25. Lynch, S. Discussion of Some Recent Literature on Hydrogen-Embrittlement Mechanisms: Addressing Common Misunderstandings. *Corros. Rev.* **2019**, *37*, 377–395. [CrossRef]
26. Madelen, O.; Todoshchenko, I. *Hydrogen Effects on Austenitic Stainless Steels and High-Strength Carbon Steels*; School of Engineering, Aalto University: Helsinki, Finland, 2015; ISBN 9789526062051.
27. Barrera, O.; Bombac, D.; Chen, Y.; Daff, T.D.; Galindo-Nava, E.; Gong, P.; Haley, D.; Horton, R.; Katzarov, I.; Kermode, J.R.; et al. Understanding and Mitigating Hydrogen Embrittlement of Steels: A Review of Experimental, Modelling and Design Progress from Atomistic to Continuum. *J. Mater. Sci.* **2018**, *53*, 6251–6290. [CrossRef]
28. Djukic, M.B.; Zeravcic, V.S.; Bakic, G.; Sedmak, A.; Rajicic, B. Hydrogen Embrittlement of Low Carbon Structural Steel. *Procedia Mater. Sci.* **2014**, *3*, 1167–1172. [CrossRef]
29. Nagumo, M. Hydrogen Related Failure of Steels—A New Aspect. *Mater. Sci. Technol.* **2004**, *20*, 940–950. [CrossRef]
30. Koyama, M.; Akiyama, E.; Lee, Y.K.; Raabe, D.; Tsuzaki, K. Overview of Hydrogen Embrittlement in High-Mn Steels. *Int. J. Hydrogen Energy* **2017**, *42*, 12706–12723. [CrossRef]
31. Birnbaum, H.K.; Sofronis, P. Hydrogen-Enhanced Localized Plasticity-a Mechanism for Hydrogen-Related Fracture. *Mater. Sci. Eng. A* **1994**, *176*, 191–202. [CrossRef]
32. Bak, S.H.; Abro, M.A.; Lee, D.B. Effect of Hydrogen and Strain-Induced Martensite on Mechanical Properties of AISI 304 Stainless Steel. *Metals* **2016**, *6*, 169. [CrossRef]
33. Bak, S.H.; Kim, S.S.; Lee, D.B. Effect of Hydrogen on Dislocation Structure and Strain-Induced Martensite Transformation in 316L Stainless Steel. *RSC Adv.* **2017**, *7*, 27840–27845. [CrossRef]
34. Yoshioka, Y.; Yokoyama, K.; Sakai, J. Role of Dynamic Interactions between Hydrogen and Straininduced Martensite Transformation in Hydrogen Embrittlement of Type 304 Stainless Steel. *ISIJ Int.* **2015**, *55*, 1772–1780. [CrossRef]
35. Izawa, C.; Wagner, S.; Deutges, M.; Martín, M.; Weber, S.; Pargeter, R.; Michler, T.; Uchida, H.H.; Gemma, R.; Pundt, A. Relationship between Hydrogen Embrittlement and Md30 Temperature: Prediction of Low-Nickel Austenitic Stainless Steel's Resistance. *Int. J. Hydrogen Energy* **2019**, *44*, 25064–25075. [CrossRef]

36. Hardie, D.; Butler, J.J.F. Effect of Hydrogen Charging on Fracture Behaviour of 304L Stainless Steel. *Mater. Sci. Technol.* **1990**, 6. [CrossRef]
37. Tsay, L.W.; Yu, S.C.; Huang, R.T. Effect of Austenite Instability on the Hydrogen-Enhanced Crack Growth of Austenitic Stainless Steels. *Corros. Sci.* **2007**, *49*, 2973–2984. [CrossRef]
38. Wang, S.; Martin, M.L.; Sofronis, P.; Ohnuki, S.; Hashimoto, N.; Robertson, I.M. Hydrogen-Induced Intergranular Failure of Iron. *Acta Mater.* **2014**, *69*, 275–282. [CrossRef]
39. Martin, M.L.; Robertson, I.M.; Sofronis, P. Interpreting Hydrogen-Induced Fracture Surfaces in Terms of Deformation Processes: A New Approach. *Acta Mater.* **2011**, *59*, 3680–3687. [CrossRef]
40. Laureys, A.; Depover, T.; Petrov, R.; Verbeken, K. Microstructural Characterization of Hydrogen Induced Cracking in TRIP-Assisted Steel by EBSD. *Mater. Charact.* **2016**, *112*, 169–179. [CrossRef]

Disclaimer/Publisher's Note: The statements, opinions and data contained in all publications are solely those of the individual author(s) and contributor(s) and not of MDPI and/or the editor(s). MDPI and/or the editor(s) disclaim responsibility for any injury to people or property resulting from any ideas, methods, instructions or products referred to in the content.